Higher-Order Structure of Polymyxin B: The Functional Significance of Topological Flexibility

Martha D. Bruch,*,† Yolanda Cajal,‡,§ John T. Koh,‡ and Mahendra K. Jain‡

Contribution from the Department of Chemistry and Biochemistry, University of Delaware, Newark, Delaware 19716, and Chemistry Department, State University of New York at Oswego, Oswego, New York 13126

Received July 8, 1999. Revised Manuscript Received October 18, 1999

Abstract: The higher order structure of antibacterial polymyxin B (PxB), an N-acylated pentacationic (4−10)-cyclic decapeptide, is determined from NMR data by simulated annealing calculations. The antibacterial selectivity of PxB against Gram-negative organisms suggests that PxB must participate in specific microscopic interactions with these organisms, and the structure of PxB provides insights into these interactions. Significance of the topological flexibility of certain parts of the structure in relation to the membrane-mimetic environment is developed to suggest the presence of two distinct and specific phosphoester binding sites per PxB. Although disordered in water, PxB remains in a monomeric form and adopts a well-defined structure in aqueous trifluoroethanol (TFE). Circular dichroism results show a comparable structure in aqueous TFE and on anionic vesicles. Docking and energy minimization calculations show that the two phosphoester binding sites are essentially on the same face of the structure. The topology of the ring is locked in a fixed relationship between residues 6, 7, and 10. However, the pucker of the ring changes residues 4 and 5 on one side and residues 8 and 9 on the other side. The structural flexibility within the NMR constraints permits occupancy of the sites individually or simultaneously, in a 10 to 14 Å range for the phosphorus-to-phosphorus distance between the two sites. Thus, for interactions at the Gram-negative cell surface, a PxB molecule could not only bind to the headgroup of one or two phosphatidylglycerols, but remarkably, the two sites could also simultaneously accommodate the 1,4′-diphosphodiglucosamine of lipid A backbone of a lipopolysaccharide. The observed combination of both fixed and flexible regions of PxB, referred to as higher order structure, accounts for its ability to perform a range of microscopically distinct functions guided by the local environment at the bacterial cell surface.

Introduction

As many of our current antimicrobial strategies succumb to resistant strains under clinical situations, it is imperative that we learn from the evolutionary successes of the alternative strategies found in nature. Cationic peptide antimicrobials are ubiquitous across the whole range of flora and fauna.[1] Polymyxins, as a prototypical example, produced by the Gram-positive *Bacillus* species, are selective and potent antimicrobials against Gram-negative organisms.[2] Polymyxin B (PxB) has been in clinical use for several decades, but it has only recently been established that cationic peptide antibacterials such as PxB induce a highly selective cellular stress that interferes with hyperosmotic response and leads to stasis and cell death.[3] For its Gram-negative selectivity, PxB must promote its own self-uptake into the periplasmic space by breaching the lipopolysaccharide layer and interact in a precise manner with phospholipid interfaces in the periplasmic space.[2,4] The chain of events in this novel antibacterial mechanism poses a question: How does a small peptide carry out a set of diverse functions with such a remarkably high degree of structural specificity? Although chemists have begun to rise to the challenge of synthesizing molecules that mimic some of these functions,[5] a better understanding of the structure and molecular behavior of PxB would enable rational design of synthetic analogues.

Insights into the molecular basis for the antibacterial stress caused by PxB can be gained by investigation of the three-dimensional structure of the peptide. Unfortunately, PxB, a decapeptide with an acyl chain (Figure 1), is disordered in water and has also eluded crystallization. Furthermore, previous NMR studies have failed to yield sufficient information to enable the determination of a three-dimensional structure of PxB.[6] However, circular dichroism (CD) results indicate that trifluoro-

* To whom correspondence should be addressed. Telephone: 315-341-2675. FAX: 315-341-5424. E-mail: bruch@oswego.edu.

† SUNY at Oswego.

‡ University of Delaware.

§ Current Address: Department de Fisicoquimica, Universitat de Barcelona.

(1) Hancock, R. E. W.; Falla, T.; Brown, M. *Adv. Microbiol. Physiol.* **1995**, *37*, 135−175.

(2) Storm, D. R.; Rosenthal, K. S.; Swanson, P. E. *Annu. Rev. Biochem.* **1977**, *46*, 723−763.

(3) (a) Oh, J.-T.; Van Dyk, T. K.; Cajal, Y.; Dhurjati, P. S.; Sasser, M.; Jain, M. K. *Biochem. Biophys. Res. Comm.* **1998**, *246*, 619−623. (b) Oh., J.-T.; Cajal, Y.; Dhurjati, P. S.; Van Dyk, T. K.; Jain, M. K. *Biochim. Biophys. Acta* **1998**, *1415*, 235−245. (c) Oh, J. T.; Cajal, Y.; Skowronska, E. M.; Belkin, S.; Chen, J.; Van Dyk, T. J.; Sasser, M.; Jain, M. K. *Biochim. Biophys. Acta* **2000**, in press. (d) Liechty, A.; Chen, J.; Jain, M. K. *Biochim. Biophys. Acta* **2000**, in press.

(4) Cajal, Y.; Berg, O. G.; Jain, M. K. *Biochem. Biophys. Res. Commun.* **1995**, *210*, 746−752

(5) (a) Li., C.; Budge, L. P.; Driscoll, C. D.; Willardson, B. M.; Allman, G. M.; Savage, P. B. *J. Am. Chem. Soc.* **1999**, *121*, 931−940. (b) Li, C.; Lewis, M. R.; Gilbert, A. B.; Noel, M. D.; Scoville, D. H.; Allman, G. W.; Savage, P. B. *Antimicrob. Agents Chemother.* **1999**, *43*, 1347−1349.

(6) Bhattacharjya, S.; David, S. A.; Mathan, V. I.; Balaram, P. *Biopolymers* **1997**, *41*, 251−265. (b) Perkins, S. J.; Radda, G. K.; Richards, R. E. *Eur. J. Biochem.* **1978**, *82*, 551−561.

10.1021/ja992376m CCC: $18.00
Published on Web 12/10/1999

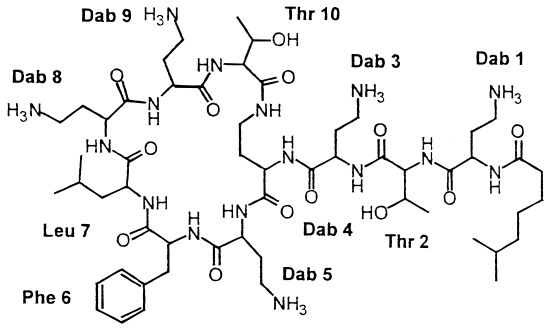

Figure 1. Primary structure of polymyxin B (PxB) PxB is a peptide containing 10 amino acids with the primary structure indicated by the three-letter code for amino acids, and Dab is 1,3-diamino butyric acid. Dab-4 has an additional amide linkage between its 3-amino group and the C-terminal carboxylate of Thr-10 to form a cycle. The N terminus of Dab-1 is end-capped with a long alkyl chain.

ethanol (TFE) induces a conformational change in PxB which is similar to the change observed at phospholipid interfaces.[7] Since CD cannot provide residue-specific details of the structure or dynamics of the peptide, we have characterized the structural preferences of PxB using two-dimensional nuclear magnetic resonance (2D NMR) in combination with simulated annealing and molecular modeling calculations. The results reveal novel and functionally significant features of the higher order structure: a part of the PxB molecule, comprised primarily of residues 6, 7, and 10, remains in a remarkably stable conformation that is conserved over a range of TFE concentrations, and the remainder of the (4−10)-ring is more flexible. However, simulated annealing calculations show that locking residues 6, 7, and 10 effectively constrains both sides of the ring, and this limits the flexibility primarily to variations in the ring pucker. This combination of well-defined fixed and flexible regions, which we refer to as higher-order structure, may be significant for the range of molecular interactions of PxB at phospholipid interfaces[7] where a more restricted single geometry may not be adequate.

The significance of the variation in ring pucker in terms of the binding to phosphoester groups is further examined using molecular simulations. These calculations suggest that ordered PxB structures contain two distinct binding sites for anionic phosphoester groups. Furthermore, changes in backbone conformation and ring pucker of PxB are observed when the substituents on the phosphoester groups are varied collectively. The backbone flexibility of PxB and variation in ring pucker accommodates the necessary range of geometry required for both the binding of intramolecular phosphates of lipid A and the binding of two phosphatidylglycerol molecules to PxB. These results suggest a model whereby an ordered structure with localized flexibility could allow PxB to sample the range of conformational space necessary to engage in the complex set of molecular interactions required for its antibacterial action.

Results and Discussion

Figure 2 shows characteristic changes in the CD spectrum of PxB which suggest that the peptide adopts a more ordered structure at the interface of anionic phospholipid vesicles. At low lipid-to-peptide ratios, the primary minimum in the CD spectrum decreases in intensity and shifts from 196 to 203 nm, and a second minimum appears at 216 nm. Such changes could

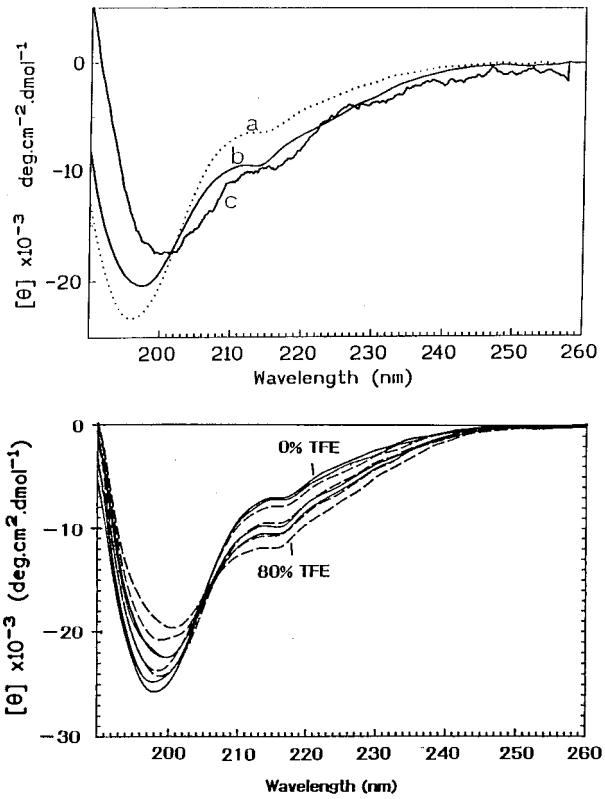

Figure 2. Circular dichroism spectra of polymyxin B**.** Top: comparison of the CD spectra of PxB in (a) 10 mM aqueous Tris buffer at pH 8, (b) 50% TFE/water (aqueous Tris buffer), and (c) DMPM (1,2-dipalmitoylphosphatidylmethanol) vesicles (7) at a vesicle:peptide ratio of 119:1. Bottom: CD spectra of 117 μM PxB in TFE/water (5 mM phosphate buffer at pH 4) at TFE concentrations of 0, 10, 20%, 30, 40, 50, 60, and 80% TFE. The spectra have an isodichroic point at 205 nm, which suggests a two-state transition from a random structure to a more ordered structure in TFE.

form the structural basis for the binding of PxB to anionic vesicles and the formation of vesicle-vesicle contacts; PxB does not bind to zwitterionic vesicles.[7] Similar intensity changes as well as a red shift are also observed in the CD spectrum upon addition of TFE to aqueous solutions of PxB (Figure 2). These TFE concentration-dependent spectral changes are characterized by an isodichroic point at 205 nm, suggesting an equilibrium shift from a disordered to a more ordered state. The similarity in the CD spectra suggests that TFE is inducing a conformational change in PxB that is similar to that observed in anionic vesicles. Since aqueous TFE is an ideal solvent for analysis by NMR, it was chosen for structural analysis of PxB. The similarities in the CD spectra suggest that the structure of PxB in aqueous TFE is similar to the membrane-bound structure and in accord with its membrane-mimetic behavior.[8] Although the molecular dynamics of the peptide in TFE are likely to be different from the dynamics when bound to membranes, our NMR results in TFE still provide insights that aid in understanding the significant structural features of PxB on the bacterial surface.

PxB is Monomeric in Aqueous TFE Solutions. Several pieces of evidence suggest that PxB is monomeric in aqueous TFE. The CD spectrum of PxB is essentially unchanged over a concentration range from 10 μM to 1 mM. Any aggregation of

(7) (a) Cajal, Y.; Rogers, J.; Berg, O. G.; Jain, M. K. *Biochemistry* **1996**, *35*, 299−308. (b) Cajal, Y.; Ghanta, J.; Easwaran, K.; Surolia, A.; Jain, M. K. *Biochemistry* **1996**, *35*, 5684−5695.

(8) (a) Bruch, M. D.; McKnight, C. J.; Gierasch, L. M. *Biochemistry* **1989**, *28*, 8554−8561. (b) Briggs, M. S.; Gierasch, L. M. *Biochemistry* **1984**, *23*, 3111−3114. (c) Wu, C.-S. C.; Yang, J. T. *Mol. Cell. Biochem.* **1981**, *40*, 109−122. (d) Urry, D. W.; Masotti, L.; Krivacic, J. R. *Biochim. Biophys. Acta* **1971**, *241*, 600−612.

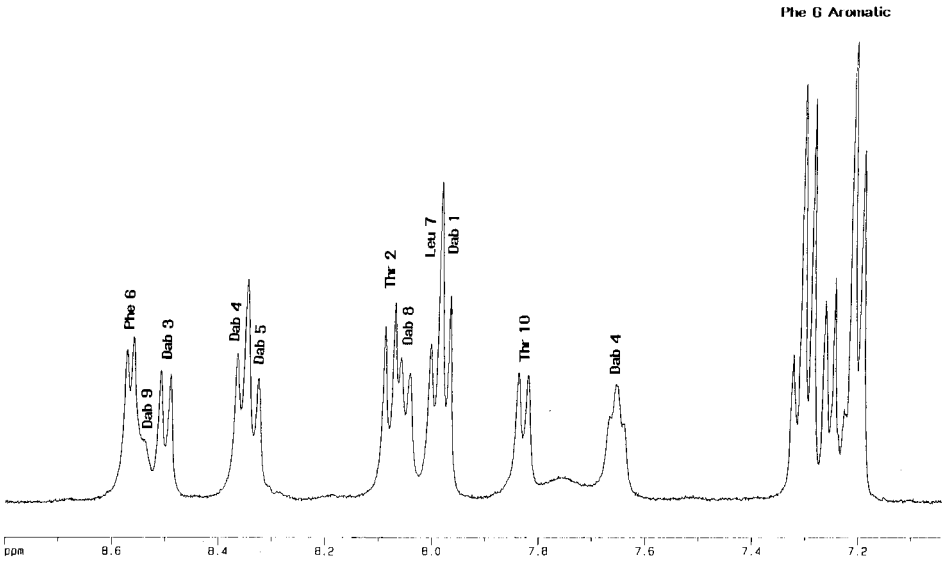

Figure 3. Amide region of the 400 MHz ^{1}H NMR spectrum of 5mM PxB in 50% TFE-d_3/pH 4 H_2O.

PxB would be affected by varying the concentration, which would probably result in a structural change reflected in the CD spectrum. The absence of changes in the CD spectrum with concentration suggests that PxB does not aggregate in this concentration range and that the observed spectral signatures are due to intramolecular rather than intermolecular aggregation. The size-exclusion chromatography in the same solvent system revealed that PxB elutes with a retention time that corresponds to the molecular weight of the monomeric form of the peptide. Also the ^{1}H NMR spectrum of 5 mM PxB in 50% TFE/H_2O (Figure 3) exhibits sharp, well-resolved resonances. The absence of line broadening suggests that no significant aggregation of PxB is occurring in TFE/H_2O solutions, which is also supported by the fact that no NOESY signals indicative of intermolecular contacts were observed.

NMR Line Assignments. CD spectra measured as a function of pH for PxB in both water and 50% TFE/H_2O showed no differences over the range of pH 2−6, and only minor changes were observed between pH 6 and 10. Furthermore, no significant functional changes are observed over a range from pH 3.5 to 9 as measured by PxB-mediated lipid exchange.[4,7] Since lowering the pH does not result in any significant structural or functional changes for PxB, the pH of all NMR samples was adjusted to 4 to facilitate water suppression using presaturation. The amide region of the 400 MHz ^{1}H NMR spectrum of PxB in 50% TFE-d_3/H_2O is shown in Figure 3. Complete line assignments, including those from the six 1,3-diamonobutyric acid (Dab) residues, were made by using the standard strategy for sequential assignments in peptides[9] and are summarized in Table 1. (See Supporting Information for spectra and experimental details).

Accessibility of Amide Protons to the Solvent. The amide/water exchange rate was estimated by dissolving the peptide in 50% TFE-d_3/D_2O and acquiring ^{1}H spectra as a function of time starting immediately after dissolution of the peptide. All but 2 of the 11 amide protons were completely exchanged with deuterium within 5 min after dissolution and were not observed in the initial proton spectrum in D_2O. Of the remaining amides, Dab-1 is fully exchanged after 12 min, while Dab-4 NH^δ is not fully exchanged until 30 min. These results indicate that all amide protons except Dab-1 NH and Dab-4 NH^δ are completely exposed to the solvent and do not participate in any intramolecular hydrogen bonds. Deuterium exchange was also probed by electrospray mass spectrometry. The sample of PxB in 50% TFE-d_3/H_2O was diluted into a large excess of D_2O, and mass spectra were taken as a function of time immediately after dilution. The change in the isotope pattern indicated that most of the deuterium exchange upon dilution into D_2O occurs within the first few minutes at pH 4, with no noticeable changes after 30 min.

Table 1. ^{1}H Chemical Shifts for PxB in 50% (v/v) TFE-d_3/H_2O at pH 4

residue[a]	NH	H^α	H^β	H^γ	H^δ
Dab-1[b]	7.98	4.56	2.05, 2.22	3.07	∼7.7
Thr-2	8.10	4.38	4.29	1.20	
Dab-3	8.51	4.52	2.12, 2.27	3.11	∼7.7
Dab-4	8.37	4.27	1.91, 2.00	3.14, 3.44	7.68
Dab-5	8.34	4.54	2.00, 2.13	2.94	7.71
D-Phe-6[c]	8.58	4.47	2.98, 3.08		
Leu-7	8.00	4.17	1.28	1.45	0.68, 0.61
Dab-8	8.06	4.30	2.25	2.14	7.76
Dab-9	8.55	4.27	2.19	3.10	∼7.7
Thr-10	7.83	4.15	4.26	1.20	

[a] Chemical shifts are measured in ppm relative to TFE at 3.88 ppm. Estimated uncertainty is ±0.02 ppm. [b] The N-terminal alkyl chain on Dab-1 has chemical shifts of 0.78, 0.80, 1.07, 1.27, 1.54, and 2.28 ppm. [c] The aromatic chemical shifts for Phe-6 are 7.21 ppm (ortho), 7.30 ppm (meta), and 7.25 ppm (para).

Temperature Dependence of the Amide Chemical Shifts. The temperature coefficients for the amide protons, measured as a change in chemical shift per degree ($\Delta\delta/\Delta T$), are at least 4.5 ppb/K for all amides except Dab-9 NH and Dab-4 NH^δ. These high temperature coefficients confirm that most amide protons are completely exposed to the solvent. The somewhat lower value of 3.5 ppb/K for Dab-4 NH^δ is consistent with the slower exchange rate for this amide proton and is indicative of partial shielding from the solvent. The value of 3 ppb/K observed for Dab-9 NH may be related to the line broadening observed for this amide, as discussed below.

Dihedral Angles and Distances Between the NH and H^α Protons. The Karplus relation between the amide vicinal coupling constant, $^3J_{HN\alpha}$, and the dihedral angle allows the angle to be estimated from the coupling constant.[10] Most amide coupling constants can be measured directly from the splitting

(9) Billeter, M.; Braun, W.; Wuethrich, K. *J. Mol. Biol.* **1982**, *155*, 321−346.

(10) Pardi, A.; Billeter, M.; Wuethrich, K. *J. Mol. Biol.* **1984**, *180*, 741−751.

Table 2. Amide Coupling Constants, $^3J_{HN\alpha}$, and Corresponding Dihedral Angles

residue	$^3J_{HN\alpha}$ (Hz)[a]	dihedral angles (deg)[b]
Dab-1	7.6	±147
Thr-2	7.4	±145
Dab-3	7.5	±146
Dab-4	6.8	±141, ±8
Dab-5	8.0	±151
Phe-6	5.0	±127, ±36
Leu-7	7.9	±150
Dab-8	7.9	±142
Dab-9	cannot measure	
Thr-10	7.3	±145

[a] Estimated uncertainty is ±0.5 Hz. [b] Dihedral angles are calculated from the Karplus relation[10].

in the 1D spectrum. However, to remove ambiguity in the case of spectral overlap, 2D *J*-resolved spectroscopy was also used to measure coupling constants,[11] and the results obtained from the 2D *J*-resolved spectrum are in good agreement with those measured from the 1D spectrum. Coupling constants could be measured for all amide protons except Dab-9 NH. Line broadening of this signal precludes measurement of this coupling constant from the 1D spectrum, and this signal is not observed in the 2D *J*-resolved spectrum. The Dab-9 NH must be involved in some sort of exchange process that does not affect the other amides. Since this exchange rate would be affected by temperature, this may also explain the anomalously low-temperature coefficient for this amide proton discussed above. Coupling constants and the corresponding dihedral angles measured for PxB in 50% TFE are summarized in Table 2.

Estimates for interproton distances were obtained by measuring cross-peak intensities in a series of two-dimensional nuclear Overhauser effect (NOESY) spectra obtained with different mixing times, ranging from 50 to 400 ms. Initial buildup rates of cross-peak volumes for individual interactions were measured, and the two-spin approximation was used to convert these buildup rates into interproton distances[12] by comparison to the rate observed for the known distance between the two nonequivalent Dab 4 H^{γ} protons, assumed to be 1.75 Å.[13] Representative distance estimates for various TFE concentrations are summarized in Table 4.

Calculated Structures for PxB in 50% TFE Despite the small size of the peptide, PxB is a challenging case for NMR analysis since 6 of the 10 amino acids are Dab residues. Since minimal spectral overlap was obtained for PxB in 50% TFE, NMR data in this solvent was used as a starting point for the generation of possible structures of PxB. Our initial objective is to obtain a set of low energy structures consistent with the NMR data. Since distance geometry algorithms often suffer from limited sampling of conformational space,[14] we chose to use restrained simulated annealing (in vacuo) to generate structures consistent with the NMR data.[15] For comparison purposes, *unrestrained* energy minimization was then performed, and these unrestrained structures have energies ranging from 160 to 188 kcal. This range of approximately 30 kcal is typical of in vacuo calculations on small, cyclic peptides such as PxB,[16] and this range makes it difficult to interpret small differences in the energies of calculated structures. Nevertheless, the lowest energy of 160 kcal probably represents a reasonable estimate for the apparent global minimum energy for purposes of comparison to other structures, and all other energies are reported relative to this apparent global minimum.

At this stage it is important to recall that the molecule is sampling a family of structures in aqueous TFE, and none of these persist in water alone. In contrast the NMR data provide information only on the *average* structure, not on the individual structures sampled. Consequently, no one structure is an adequate representation of the peptide in solution. In addition, only intraresidue and sequential restraints were used since these were the only type of NOEs observed. In fact, the absence of long-range, or even medium-range, NOEs is indicative of conformational averaging since the average long-range distance must be too long to give rise to an observable NOE. By contrast, if the molecule were locked into a rigid conformation, some long-range distances would be sufficiently short to detect in the NOESY spectrum. The absence of long-range NOEs means that the details of the tertiary structure cannot be pinpointed. Furthermore, there are few unambiguous NOEs to the Dab side chain protons due to spectral overlap, and no NOEs are observed to the alkyl chain on the N terminus, presumably because this chain is quite floppy. Consequently, the positions of the side chains and N-terminal chain are determined largely by artificial conditions inherent in in-vacuo calculations which, for flexible molecules such as PxB, tend to be biased toward maximally folded, compact conformations due to the absence of energy terms for the solvent in the force field used.[16] Despite these limitations, calculated structures based on NMR data provide valuable insights into the structural tendencies of the molecule. At the very least, structural features which are conserved among the calculated structures approximate the structural preference of the peptide, and most structures sampled by the peptide probably contain these conserved features.[17] On the other hand, for variable regions, these calculations represent a first approximation for the range of conformational space explored by the peptide. Understanding the range of possibilities for variable regions is important, since these regions represent areas where the peptide can make adjustments in response to different environments.

Due to the considerations discussed above, it is imperative to apply selection criteria carefully to eliminate unreasonable structures from the set calculated using restrained simulated annealing. Acceptable structures must meet the following criteria: (1) they must have low energy, (2) they must agree well with the NMR data, and (3) they should display Ramachandran plots with L-amino acids within the allowed regions of conformational space. Using these criteria, four of the twenty calculated structures were eliminated due to very high energy (100 kcal above the minimum) and poor agreement with the NMR data. The remaining structures fell into two categories based on the first two criteria, and these two categories will be discussed separately below. The first category includes the nine lowest-energy structures. These structures have similar energies (range of 15 kcal), and all agree well with the NMR data (Table 3), and therefore these nine structures were further examined for violations in the Ramachandran plots. One of these structures was eliminated as unreasonable because Dab-9 had φ/ψ angles

(11) Aue, W. P.; Karhan, J.; Ernst, R. R. *J. Chem. Phys.* **1976**, *64*, 4226−4227.
(12) (a) Clore, G. M.; Gronenborn, A. M. *J. Magn. Reson.* **1985**, *61*, 158−164. (b) Dobson, C. M.; Olejniczak, E. T.; Poulsen, F. M.; Ratcliffe, R. G. *J. Magn. Reson.* **1982**, *48*, 97−110.
(13) Braun, W.; Bosch, C.; Brown, L. R.; Go, N.; Wuethrich, K *Biochim. Biophys. Acta* **1981**, *667*, 377−396.
(14) Metzler, W. J.; Hare, D. R.; Pardi, A. *Biochemistry* **1989**, *28*, 7045−7052.
(15) Nilges, M.; Clore, G. M.; Gronenborn, A. M. *FEBS Lett.* **1988**, *229*, 129−136.
(16) Rizo, J.; Koerber, S. C.; Bienstock, R. J.; Rivier, J.; Gierasch, L. M.; Hagler, A. T. *J. Am. Chem. Soc.* **1992**, *114*, 2860−2871.
(17) Glaser, R. W.; Grune, M.; Wendelt, C.; Ulrich, A. S.; *Biochemistry* **1999**, *38*, 2560−2569.

Table 3: Energies and Violations for Low-Energy Structures

motif[a]	energy[b] (kcal)	forcing[c] (kcal)	no. dihedral angle[d] violations (>5°)	no. distance (>0.1 Å)	violations[e] (>0.2 Å)	no. residues outside most favored region[f]
A	20.1	2.7	0	4	0	2
A	27.9	4.4	0	3	0	2
A	31.6	5.7	2	5	0	3
A′	20.6	3.1	0	4	0	2
B	22.5	3.5	0	3	0	2
B	32.1	5.6	0	4	0	2
B′	35.7	4.7	0	5	0	3
C	23.2	5.7	1	6	1	4

[a] A, B, C refer to the motifs represented by Figure 4A, B, and C, respectively. A′ is similar to A except for Dab-4, while B′ is similar to B except for Thr-2. [b] Energies are relative to the apparent global minimum of 160 kcal. [c] Additional contribution to the energy due to the penalty term associated with violations of distance and angle restraints. [d] A total of nine angle restraints were used. [e] A total of 58 distance restraints were used. [f] The number of L-amino acids outside the most favored regions of the Ramachandran plot, not including the N- and C-terminal residues.

in a disallowed region of the Ramachandran plot. The remaining eight low-energy structures had no L-residues in disallowed regions, and therefore these eight structures represent the desired set of reasonable structures consistent with the NMR data (Table 3).

These eight structures fall into several groups, represented by the three structures shown in Figure 4. Although variation in structure is evident, certain features are conserved. The overall structure is quite flat, with the aromatic ring oriented over the leucine methyl groups, and with a kink between residues 1−3 in the linear part of the peptide. However, differences in the ring pucker are evident, and changes in the ring pucker also affect other parts of the molecule. The three structures shown in Figure 4 represent three different motifs that were observed among the eight low-energy structures. The lowest-energy structure (4A) had all L-amino acids either inside or on the border of the most favored regions of the Ramachandran plot. Two other structures were obtained with a similar appearance and similar Ramachandran plots, and a fourth structure (designated A′ in Table 3) is similar except for a difference in the geometry of Dab-4. A second motif, represented by Figure 4B, was observed for two other calculated structures. A third structure (designated B′ in Table 3) is quite similar to these two except that Thr-2 is in a more extended conformation. Structures designated B or B′ had some residues further outside the most favorable regions of the Ramachandran map, but all were well within the allowed regions. Finally, a unique structure was obtained, as shown in Figure 4C. This structure had more distance and angle violations as well as more residues outside the most favored regions, so that this structure is probably less reliable than the other two motifs.

The lowest-energy structures for the three structural motifs described above are essentially isoenergetic, with a total range of only 3.1 kcal (Table 3). The observation of several dominant motifs in combination with the flexibility of this small peptide suggests that the peptide is interconverting among these possibilities. Changes in the ring pucker among the structures involves flipping residues 4, 8, and 9 while holding residues 6, 7, and 10 in a relatively constant position in space. If this type of interconversion were occurring in solution, the Dab-9 amide proton would flip between two very different environments. This type of exchange could explain the selective line broadening observed for Dab-9 NH. As mentioned earlier, the alkyl chain on the N terminus of the molecule is extremely floppy; only one NOE is observed to this chain. Presumably, the NOEs are vanishingly small for the "tail" due to extensive molecular motion.

As a further test, these eight structures were examined to see if any NOEs are predicted that are not observed experimentally. Some structures predict NOEs to Dab-1 NH that are not observed, but these NOEs are probably vanishingly small due to the extensive motional averaging of the N-terminal alkyl chain discussed above. All structures predict a NOE between Dab-9 H^{α} and Thr-10 NH which is not observed. This may be due to motional averaging associated with the unusual behavior of Dab-9 discussed earlier. In any case, all structures have the same expected distance of 3.58 ± 0.02 Å between these protons; therefore, the absence of this NOE is not a basis for selecting for or against any of these structures.

The second category includes the remainder of the 20 structures calculated using the protocol described earlier. These seven structures have somewhat higher energies (+40 to +60 kcal above the minimum) with larger distance and angle violations than the structures represented in Figure 4. Much more variability is observed for these structures than with the lower-energy structures discussed above. These structures represent a greater range of conformations which may be visited by PxB, and they may represent transitional structures visited between the main conformers shown in Figure 4. The higher energy and larger number of violations suggest that these structures have a smaller solution population than the structures shown in Figure 4, but the energetic balance could change with altered environmental constraints (see below).

The local dynamics of the peptide were probed further by comparison of the dihedral angles obtained from the amide vicinal coupling constants to the intraresidue distances between the amide and H^{α} protons, obtained from the NOE data. For L-amino acids in a rigid conformation, the relationship between the dihedral angle and the interproton distance is known.[18] However, due to the inverse sixth power dependence of the NOE on the interproton distance, in the case of motional averaging, the average distance obtained from NOE measurements is heavily weighted toward the shortest distance sampled. Consequently, coupling constants are averaged differently by molecular motion than are NOE measurements. Discrepancies between the NH/H^{α} distance and the corresponding dihedral angle are indicative of motional averaging. In PxB, amide coupling constants for L-amino acid residues 1, 2, 3, 5, 7, 8, and 10 are all between 7.3 and 8 Hz, and, in the absence of motional averaging, the corresponding dihedral angle is consistent with a distance of 2.8 Å.[18] The measured NH/H^{α} distance of the linear segment 1−3 and of residue 7 is indeed 2.8 Å, and this is consistent with the earlier statement that the orientation of the (1−3)-segment, and the part of the ring involving residues 6 and 7, is relatively rigid with a conserved conformation. By contrast, the interproton distances measured for residues 5, 8, and 10 are much shorter (2.5, 2.4, and 2.5 Å, respectively), and this is consistent with motional averaging associated with variation in ring pucker.

Effect of Changing the Solvent. Additional insight into the effect of the environment on the conserved structural features is provided by the NMR data at varying TFE content. In a polypeptide chain, the H^{α} chemical shifts are primary indicators of secondary structure,[19] and the H^{α} shifts of most residues in

(18) Wuethrich, K. *NMR of Proteins and Nucleic Acids*, John Wiley and Sons: NY, 1986.

(19) Wishart, D. S.; Sykes, B. D.; Richards, F. M. *Biochemistry* **1992**, *31*, 1647−1651.

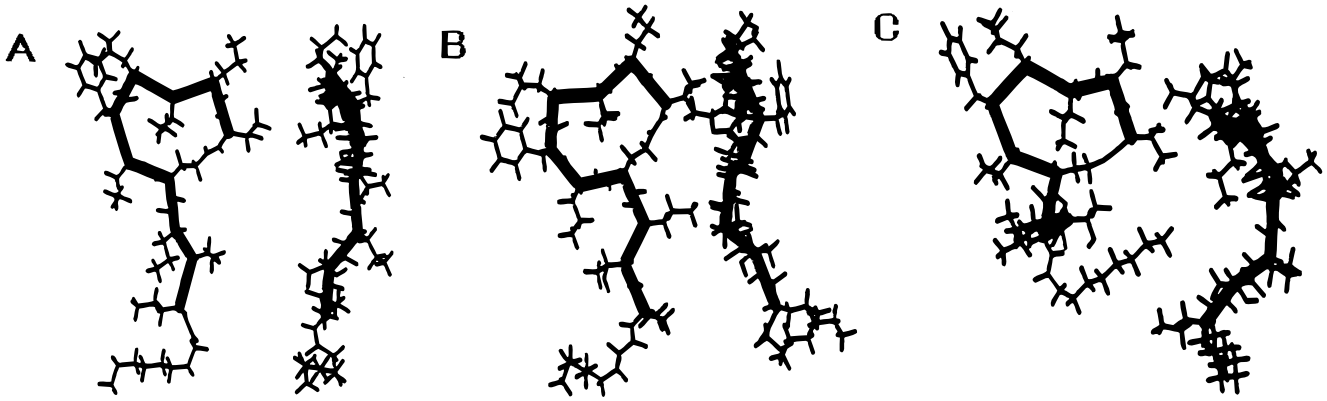

Figure 4. Three representative structures of PxB obtained from simulated annealing in combination with NMR data obtained in 50% TFE/H_2O. All structures illustrate the absence of a pore in the ring (top view), and the planar nature of the molecule (side view). The lowest-energy structural motif (A) was obtained four times, motif (B) was obtained three times, and motif (C) was obtained only once.

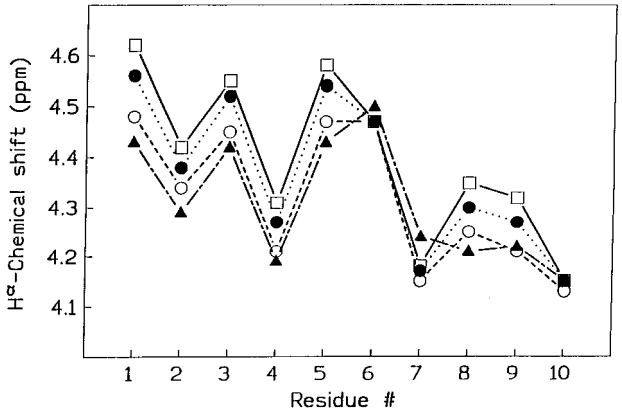

Figure 5. 400 MHz H^α chemical shifts for each residue of 5.5 mM PxB in 0, 30, 50, and 70% TFE (by volume in pH 4 H_2O), respectively. Chemical shifts of PxB in (▲) water, (○) 30% TFE, (●) 50% TFE, and (□) 70% TFE.

PxB increase systematically as the TFE concentration is increased from 0 to 70%, as shown in Figure 5. These changes in H^α shifts reflect the conformational changes observed in the CD spectra (Figure 2). However, the H^α shifts for Phe-6, Leu-7, and Dab-10 are essentially invariant with changes in TFE content. This invariance suggests that certain conformational features involving these residues are conserved. For example, a strong NOE between the Phe-6 aromatic ring and the Leu-7 methyl groups was observed in all cases, indicating that the aromatic ring is always situated over these methyl groups. Dab-10 represents an interesting case since its H^α chemical shift is invariant with changes in TFE content, which suggests a fixed conformation associated with this residue, but the NH/H^α distance is shorter than expected based on the amide coupling constant, which suggests motional averaging. We attribute this difference to the possibility that the NH/H^α bond of this residue serves as a pivot point or "hinge" for changes in the ring pucker.

To understand the nature of the conformational change with increasing TFE content, the same protocol that was used to generate structures consistent with the NMR data in 50% TFE was applied to the NMR data in both 30 and 70% TFE. Due to spectral overlap, fewer restraints were available for each of the latter two cases compared to 50% TFE data, and thus the structures for 30 and 70% TFE are not as well defined. Nonetheless, many distances could be measured in all three cases, and these distances are summarized in Table 4. Some of these distances are essentially unchanged in the three solvents, reflecting conserved conformational features. However, variation in the NH/NH distances with the TFE content is indicative of changes in the ring pucker. There also are significant changes in distances to the Leu-7 methyl groups, which reflects a change in side chain orientation. No significant variation in coupling constants is observed as the TFE content is changed; therefore, the average dihedral angles are invariant.

Table 4. Selected Interproton Distances for PxB in Different TFE Content (v/v) at pH 4.0

distance (Å) (± 10%)	30% TFE	50% TFE	70%TFE
Dab-4 NH/Dab-4 NH^δ	3.8	3.8	3.5
Dab-4 NH^δ/Thr-10 NH	3.8	3.1	3.4
Dab-9 NH/Thr-10 NH	3.7	2.9	3.0
Leu-7 NH/Phe-6 NH	3.7	4.0	3.4
Phe-6 NH/Phe-6 ortho	3.9	3.9	4.1
Leu-7 NH/Phe-6 ortho	3.5	3.4	3.7
Leu-7 H^α/Dab-8 NH	2.5	2.7	2.6
Thr-10 H^α/Dab-4 NH^δ	2.3	2.4	2.2
Leu-7 H^α/Leu-7 NH	2.6	2.8	2.7
Thr-10 H^α/Thr-10 NH	2.4	2.5	2.6
Phe-6 H^α/Phe-6 ortho	2.7	2.7	2.7
Phe-6 ortho/Leu-7 CH_3	3.2,3.3	3.5,3.6	2.9,3.6
Phe-6 meta/Leu-7 CH_3	3.3,3.6	3.4,3.7	3.0,3.7
Dab-4 NH^δ/Dab-4 H^γ	2.2,2.2	2.4,2.4	2.2,2.5
Dab-4 NH/Dab-4 H^γ	2.7,2.8	2.9,2.9	2.6,2.6
Dab-4 NH^δ/Thr-10 CH_3	3.6	3.9	3.5
Thr-10 NH/Thr-10 CH_3	2.8	3.2	2.7
Thr-2 NH/Thr-2 CH_3	3.1	3.3	2.9
Leu-7 NH/Leu-7 CH_3	2.6, 3.6	2.7, 3.2	2.5,2.9
Leu-7 H^α/Leu-7 CH_3	2.4,3.0	2.4, >4	2.3, >4

Although more variation is observed for the 30 and 70% TFE structures, the lowest-energy structure in both cases is similar to the lowest-energy structures obtained for 50% TFE, with differences primarily in the ring pucker. Moreover, the energies of the lowest-energy structures are nearly the same, with energies of +24, +20, and +28 kcal for 30, 50, and 70% TFE, respectively. These results suggest that the changes observed in the CD spectra are primarily due to changes in the average ring pucker and side chain orientations, with more compact structures favored at high TFE content.

Simulation of the Binding of Phosphodiester Group to PxB. The structure and properties of PxB represent a prototype for understanding a ubiquitous and evolutionarily successful antibacterial strategy. A novel locus for the antibacterial stress by this class of cationic peptides has emerged only recently. The basis for the primary antibacterial stress[3] is attributed to the ability of the peptides to form contacts between phospholipid interfaces.[7] For example, sublethal concentrations of PxB in growing *Escherichia coli* induce a stress whose end result is

transcription of *osmY* and *micF* genes, without any effect on the transcriptional responses related to the loss of proton gradient, oxidative damage, or perturbation of macromolecular synthesis.[3] The *osmY* gene is normally expressed during the stationary phase, and the same response is also associated with hyperosmotic stress induced by NaCl and sucrose,[20] two commonly used food preservatives. Remarkably, these antibacterial peptides also interfere with the very rapid shrinkage of the cytoplasmic compartment in response to hyperosmotic shock.[3b] On the basis of independent biophysical evidence,[7] these observations suggest that PxB forms contacts between the two phospholipid interfaces surrounding the periplasmic space. As discussed below, the higher-order structure deduced from NMR data is useful for refining this hypothesis with the suggestion that the primary functionally relevant interaction of PxB is with phosphoester groups at the membrane/water interfaces.

The size of the pore formed by the ring segment of PxB (residues 4−10) is large enough to bind an anion like chloride or phosphate, but it is unlikely to be an ionophore or a channel for a small anion because the passage is blocked by the side chain of Dab-8 (Figure 4). Even if the side chain could swing out to clear the passage, the outer surface of the ring that would have to form a contact with the acyl chains in the bilayer is not hydrophobic, nor is the stacked structure likely to form a channel with a hydrophobic surface. This interpretation is supported by the fact that leakage of anionic vesicles is not seen in the presence of PxB unless the mole fraction of the peptide is >3% to induce a detergent like disruption of the bilayer.[3,7]

It is generally agreed that the disruption of the outer membrane is a necessary, but not sufficient, condition for the antimicrobial action of PxB on Gram-negative organisms.[2,5,21,22] PxB is not antibacterial against Gram-positive organisms. Lysis is also ruled out for the antibacterial effect on *E. coli*[3]. Furthermore, PxB does not cause leakage or lysis of anionic vesicles,[7] while polylysine and other lytic cationic peptides do not show the specific effects of PxB. In terms of our hypothesis outlined earlier, at least two types of interactions occur between cationic PxB and anionic phosphoester groups. First of all, the self-promoted uptake of PxB from the growth medium into the periplasmic space of a Gram-negative organism requires a disruption of the outer membrane barrier. Here the primary interaction would be through the 1- and 4′-phosphates on the sugar backbone of the lipid A portion of the lipopolysaccharide. Second, PxB forms contacts in the periplasmic space between the anionic phospholipid containing outer surface of the cytoplasmic membrane and the inner surface of the outer membrane. Both the conditions must be fulfilled for the antibacterial action[3,21] This requires PxB to interact with both mono- and dianionic phosphoesters. On the basis of these observations we surmise that PxB-mediated contacts between the two phospholipid interfaces surrounding the periplasmic space is a necessary condition for the antibacterial effect on Gram-negative organisms.[3,4] As developed below, in this model, the structural flexibility involving residues 4, 8, and 9 is relevant for the multiplicity of interactions encountered by PxB with the lipidic targets as the basis for its antimicrobial action.

Certain related observations serve as useful controls for our hypothesis that the phosphoester binding sites on PxB are made up largely from the (3−10)-segment of PxB. PxB-nonapeptide, containing residues 2 through 10 of PxB but without the alkyl chain, interacts with lipopolysaccharide and disrupts the outer membrane. Yet the nonapeptide is neither antimicrobial nor capable of inducing the hyperosmotic stress[3] or mediating the vesicle-vesicle contacts.[7] On the other hand, octapeptin, with residues 3−10 of PxB and an acyl chain at the N terminus, is antibacterial[2] and promotes vesicle-to-vesicle exchange of monoanionic phospholipids.[7] Since octapeptin shows all the functions of PxB, it appears only four charges, Dab-3, −5, −8, and −9 are functionally significant, although Dab-1 may also contribute. Since the inactive nonapeptide also contains these four charges, their presence appears to be a necessary, but not a sufficient, condition for antimicrobial activity.

Under physiological conditions, most phosphoester groups contain one or two anionic charges, so that there are at least two potential binding sites on PxB. In the absence of detailed knowledge of the structure of PxB at the interface or in membrane−membrane contacts, we resort to modeling potential interactions between PxB and several anionic phosphoesters (Table 5). The NMR structure in TFE was used as a starting point for such simulations because the CD signatures are similar to those seen on phosphatidylglycerol vesicles. A Monte Carlo docking search of the entire surface suggested that PxB contains two sites that have significant binding affinity for phosphodiester groups. On the basis of docking experiments of a variety of phosphoester ligands, two well-defined sites emerge: site A is made up of the positively charged amino groups of Dab-1, Dab-3, and Dab-5, and site B is on the puckered ring face formed with the amino groups of Dab-8, Dab-9, and H-bonding contributions from NH and OH of Thr-10. The two sites are separated by the 4−10 bridge that completes the ring. They remain separate and independent despite variation in the ring pucker caused by molecular motion because the fixed structure of residues 6 and 7 on one side and residue 10 on the other side of the ring restricts the range of conformational space that can be sampled by the peptide. These sites are spatially separate and distinct, and therefore they could be potentially occupied by two separate phosphate groups and/or temporally differentiated by the migration of a *single* ligand. In addition, both binding sites can accommodate two phosphoester groups in the same ligand, such as lipid A. Each of these scenarios may be critical for the antibacterial mechanism of PxB. In short, in addition to the ionic interactions, the distance, geometry, and hydrophobicity constraints of these two sites are remarkably well disposed for the desolvation of the phosphoester anions at the interface.

The calculated binding enthalpies determined in the absence of explicit solvent, using a distance-dependent dielectric, ignore the cost of desolvating the uncomplexed forms of the ligand and the receptor. Although calculations alone are not expected to accurately model the solvent and membrane interactions that occur at interfaces, the observed trends do lend insight into the significance of potential binding modes of phospholipid components and provide a basis with which to speculate about the molecular mechanism of PxB. Binding enthalpies for several phosphodiesters, docked and energy-minimized on site A or site B, are summarized in Table 5. In these calculations, the phosphoester ligand and all of the residues of PxB, except 6 and 7, were unrestrained. With the various phosphoesters, the ring pucker changes in a narrow range. This flexibility is equivalent to presenting a range of structures suggested by the NMR results. Binding enthalpies are relative to the estimated

(20) Hengge-Aronis, R. In *Eschericia Coli and Salmonella: Cellular and Molecular Biology,* 2nd ed.; Niedhardt, F. C., ed.; ASM Press: Washington, DC, 1996; pp 1497−1512.

(21) Vaara, M. *Microbiol. Rev.* **1992**, *56*, 395.

(22) Hancock, R. E. W.; Piers, K.; Brown, M.; Falla, T.; Gough, M.; Wu, M.; Fidai, S. In *Molecular Biology of Pseudomonads*; Nakazawa, T., Furukawa, K., Haas, D., Silver, S., Eds.; ASM Press: Washington, DC, 1996; pp 441−450.

Table 5. Calculated Binding Enthalpy[a] (kcal) for Phosphoesters Docked in C2-PxB or C2-Octapeptin

phosphate (charges)	site A (3/5)	site B (7/9)
HPO_4 (−3)	−54.5	−51.1
CH_3HPO_4 (−2)	−33.7	−33.0
$(CH_3)_2PO_4$ (−1)	−14.4	−19.3
glycerol-*sn*−3-phosphate (−2)	−34.7	−33.2
1,2-diacetylglycerol-*sn*−3-phosphate (−2) (= GPA)	−33.9	−33.5
GPA-monomethylester (−1) (= GPA-Me)	−17.4	−15.4
glycerol-*sn*−3-phosphoglycerol (−1)	−18.1	−20.3
4′-phosphate of lipid A (−2)	−29.9	−36.1
4′-AraN−phosphate of lipid A (−1)	−16.5	−17.1
1-phosphate of lipid A (−2)	−31.3	−33.9
lipid A with 1-P in A and 4′−P in B (P−P 11.82 A)	−54 double-docked	
lipid A with 1-phosphate in site B (P−P distance 10.92 A)	−61.7 double-docked	
two molecules of GPA (P−P distance 13.8 A)	−68.1 double-docked	
Two molecules of GPA-Me (P−P distance 13.6 A)	−32.0 double-docked	
GPA + C2-octapeptin	−26.3	−34.9
GPA-Me + C2-octapeptin	−13.6	−14.5

[a] Total estimated binding energy relative to estimated global minimum of the free ligand. Octapeptin is the 3−10 analogue of PxB with an acyl chain at the N terminus. GPA, glycerophosphatidic acid; GPA-Me- methylester of GPA; C2-octapeptin, octapeptin with an acetyl chain at the N terminus.

global minimum for the free ligand and the local minimum of the uncomplexed C2-PxB.

The large negative enthalpy of a fully charged trianionic phosphate ion docked in PxB indicates that it is the most tightly bound, and structures of lesser stability are formed with dianionic methylphosphate and monoanionic dimethylphosphate. The observed change in enthalpy of about 20 kcal/mol for each charge is substantial. The absolute magnitude of the energy with the charge suggests that the interactions are not simply distance and charge dependent (Coulombic). Additional factors must come into play, as also suggested by the fact that not all of the phosphates occupy exactly the same position in the three complexes; the side chains and the backbone residues also move appreciably to accommodate the charge and other substituents on the phosphate. This assertion is also supported by the calorimetric results discussed below.

Two phosphoester fragments of two glycerophospholipids or the two phosphoesters of lipid A can be simultaneously co-docked on PxB (Table 5). Besides the large energetic contribution associated with the number of anionic charges, modest contributions (less than 5 kcal/mol) from other interactions are apparent at the two sites. These are attributable to the formation of extra H-bonds with NH and OH of Thr-10. A change in the backbone conformation and puckering of the ring of PxB, as well as a change in the phosphoester geometry, is noticeable with a change in the substituents on the phosphoester. Interestingly, in some cases such changes seem to optimize the hydrophobic contacts. The phosphorus-to-phosphorus distance between co-docked glycerophosphates is 13.7 Å (Table 5). In this structure (Figure 6), the acyl chains extend away from PxB, suggesting that it is possible to accommodate the chains such that the PxB molecule would lie flat on the polar region of the phospholipid interface. Similarly, both the phosphates of the disaccharide headgroup of lipid A can also be co-docked on sites A and B in two different ways. In the lowest-energy structure, the 4′-phosphate occupies site A with a phosphorus-to-phosphorus distance of 10.9 Å. However, we prefer the structure with a somewhat higher energy in which the 1-phosphate occupies site A with the phosphorus-to-phosphorus distance of 11.8 Å. In this structure, the hydrophobic contacts between the two sites are clearly aligned (Figure 7). Together, these interconvertible co-docked structures suggest a possible mode of binding of PxB to the lipopolysaccharide on the bacterial outer membrane for self-uptake, as well as during the contact formation between phosphatidylglycerol interfaces. On the basis of the constraints of the interfaces involved in these processes, we suspect that other structural forms of the complexes must also exist, at least transiently, on the interfaces. All such considerations place a demand on the relative position and orientation of the two phosphoester binding sites on PxB. Yet another consequence of the interaction with lipid A is that a 4′-aminoarabinose substitution destabilizes the structure significantly (Table 5), which may provide a rationale for the fact that bacteria containing such a modification in their lipopolysaccharide are resistant to the uptake of PxB.[23]

There is an interesting feature to the structures in Figures 6 and 7. The hydrophobic regions, the acyl chain at the N terminus and patch of residues Phe-6/Leu-7, are well-separated by the 4−10 bridge between the two binding sites. How this structure relates to PxB-contacts that mediate direct vesicle-to-vesicle exchange of phosphatidylglycerol[7] remains to be modeled. However, it is likely that if PxB complex with two monoanionic phospholipids lies on the interface, the exposed hydrophobic regions could provide a hydrophobic drive for a close apposition of the two-vesicle surface. Such a hydrophobic region in the PxB-contact between interfaces would be critical not only for the stability of the contact but also for the phospholipid exchange, where the acyl chains must be protected from the aqueous phase during the transit from one interface to the other. Support for this possibility is provided by the fact that the Phe-6/Leu-7 hydrophobic motif is highly conserved in the various polymyxins and that the presence of a medium-length acyl chain is critical for the antibacterial and phospholipid exchange functions.

Additional insights can be gained by comparing our results on PxB with NMR results reported on the inactive nonapeptide.[6a] When docked to lipid A, the nonapeptide adopts a relatively rigid conformation that has some of the same structural features that are conserved in our PxB structures. In particular, in both PxB and the nonapeptide, the aromatic ring of phenylalanine is in close proximity to the leucine methyl groups, forming a hydrophobic patch, similar to that discussed above for PxB, which may be critical for binding. The nonapeptide structure also has all of the carbonyl groups of the cyclic portion of the molecule on one face of the peptide, as was observed in our PxB structures. In contrast to PxB, however, the nonapeptide adopts an ordered structure in water, including intramolecular hydrogen bonds. These results imply that the inactive nonapeptide has a greater tendency to lock into one structure when compared to PxB, and this is consistent with the notion that conformational flexibility is a key feature needed for antibiotic activity. This notion is also supported by recent results on synthetic mimics of PxB.[5] These potent cholic acid-derived mimics do not share the high Gram-negative selectivity of PxB,[4] nor do they facilitate rapid lipid exchange (Jain, unpublished results). Since the analogues are quite rigid, we suggest that conformational flexibility is required to achieve both binding to the lipopolysaccharide layer *and* mediation of phospholipid exchange.

(23) Raetz, C. R. H. *Annu. Rev. Biochem.* **1990**, *59*, 129−170.

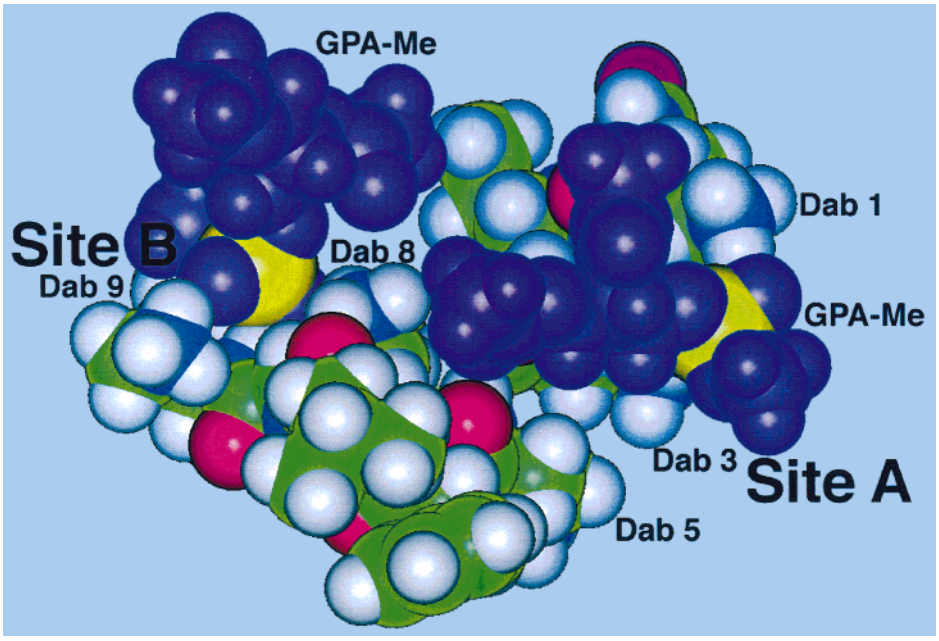

Figure 6. Proposed binding mode for two phosphatidylmethanol headgroups (1,2-diacetylglycerol-*sn*-3-phospho-methylester) to C2-PxB. The two basic sites A and B can be simultaneously occupied by phosphate ligands. See Table 4 for additional examples.

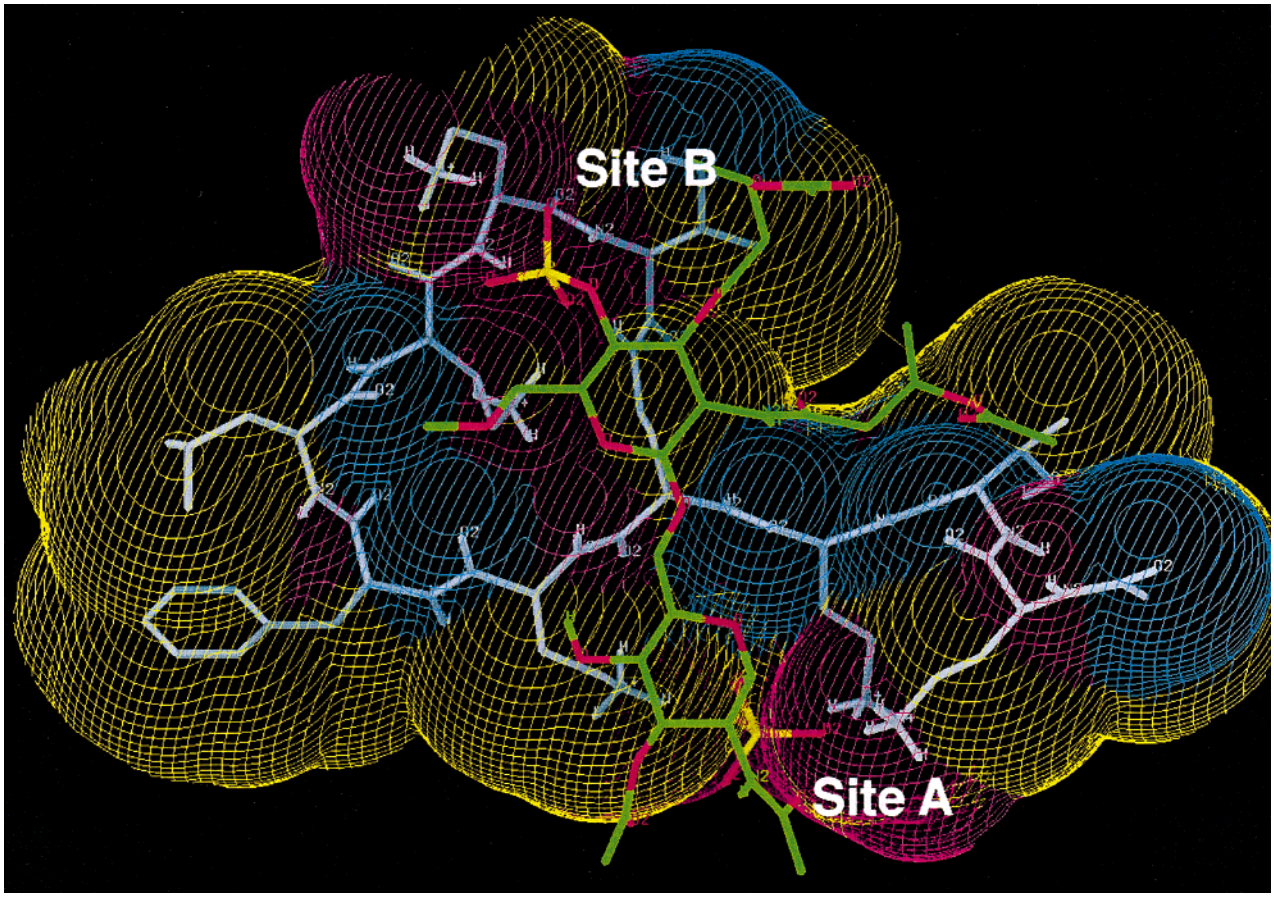

Figure 7. Proposed binding of lipid A to PxB**.** The basic sites, A and B on PxB can simultaneously bind both phosphates of the disaccharide headgroup of Lipid A. The disaccharide headgroup of lipid A superimposed on the Lee and Richards surface[29] of C2-PxB (white) shows substantial complementarity to the hydrophobic surface (yellow), the hydrogen bond donor surface (red), and the hydrogen bond acceptor surface (blue).

Heat Changes Associated with the Binding of PxB to Anionic Vesicles. The results discussed above indicate that PxB interacts quite differently with monoanionic vs dianionic lipids, and this is revealed more clearly by differences in the heat change associated with binding of PxB to mono versus dianionic phospholipid vesicles. Addition of PxB to monoanionic POPG (1-palmitoyl,2-oleoylphosphatidylglycerol) vesicles results in a rapid positive heat change, whereas the heat change with dianionic POPA (1-palmitoyl,2-oleoylphosphatidic acid) vesicles is negative, as shown in Figure 8. These results imply a significant qualitative difference in the underlying interactions of PxB with the two types of phospholipid vesicles, which may

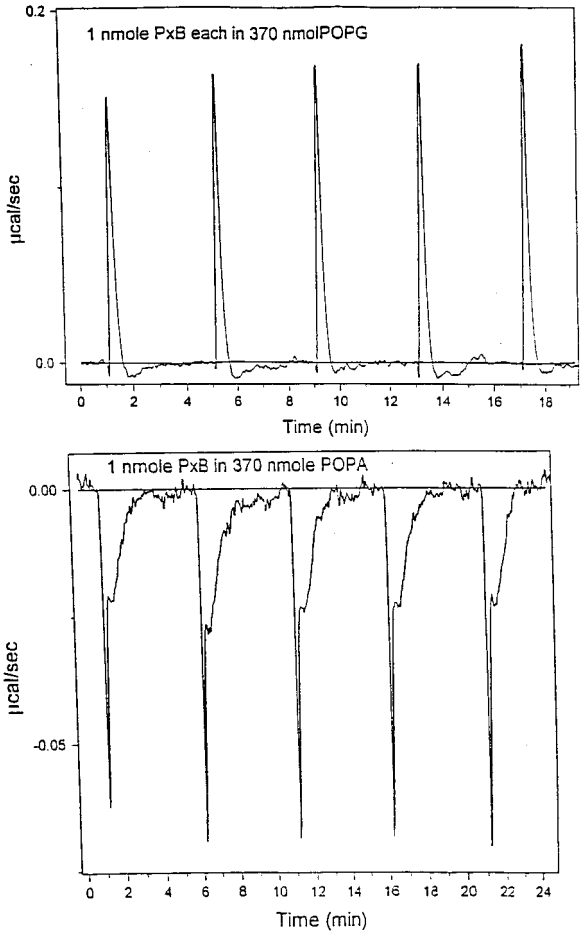

Figure 8. Heat changes associated with the addition of PxB to 0.26 mM POPG (top) or POPA (bottom) vesicles in 20 mM Tris and 40 mM NaCl at pH 8.00. The calculated apparent enthalpy change is +1.7 kcal/mol PxB for the binding to POPG, compared to a value of −2.0 kcal for the binding to POPA. Since additional changes occur at higher mole % of PxB, this method cannot be used for the determination of the binding constant.

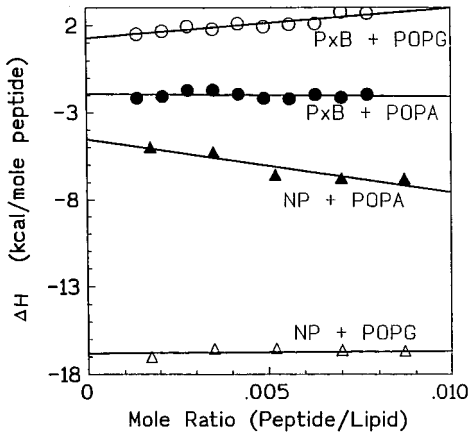

Figure 9. Heat changes associated with the titration of 0.26 mM POPG (open symbols) or POPA (closed symbols) vesicles by PxB (circles) or NP (triangles).

account for the fact that PxB mediates intervesicle exchange of POPG but not of POPA.[7] As further emphasized by results summarized in Figure 9, only the negative heat change is seen upon addition of PxB-nonapeptide to POPG or POPA vesicles.

Simple ionic interactions are expected to exhibit a negative enthalpy change, as observed for the interaction of the nonapeptide with both POPG and POPA. A negative heat change has also been reported on the binding of lipid A to PxB and NP.[24] The specificity of such ionic interactions is difficult to evaluate. On the other hand, a positive enthalpy change for the interaction of PxB with POPG (but not POPA) is only observed for the same combination of conditions under which PxB-mediated monoanionic phospholipid exchange is correlated to the antibacterial action. Consequently, we believe the positive heat change is associated with a unique feature of the peptide contacts between vesicles through which phospholipids exchange, and attribute this positive enthalpy change to a significant displacement of the phospholipid acyl chains in the PxB-mediated contacts between vesicles. Together, as suggested by molecular simulation results, the calorimetry results support the notion that the molecular changes underlying the function result from a difference in the structural forms of PxB with POPA versus POPG.

As expected from previous biophysical studies,[7] the detailed analysis of the heat change reveals a biphasic time dependence, as if the underlying process is multistep. Similarly, the peptide concentration dependence of the heat change also suggests that several different species are formed at increasing mole ratios of the peptide in phospholipid vesicles (results not shown), which precluded determination of the binding constants and associated thermodynamic quantities.

Conclusions

We suggest that the flexible topography presented by the higher-order structures of peptides may be critical for their function at interfaces. Remarkably, with a limited set of residues, PxB covers a range of conformational space for spatially and temporally restricted interactions. This may not be a property unique to PxB. For example, Glaser et al.[17] have shown that the fusogenic octadecapeptide sequence of the fertilization protein from sea urchin egg assumes a range of higher order structures in aqueous TFE which are relevant for fusion. A range of isoenergetic conformations has been suggested for mellitin,[25] which also forms vesicle-to-vesicle contacts between anionic vesicles.[26] Most of the discussion of mellitin structure has revolved around the extended helical structure which seems to account for its ability to cause leakage and disruption of zwitterionic vesicles. However, calculations using simulated annealing in the absence of solvent revealed the existence of at least five classes of conformations that are nearly isoenergetic, with a range of only 4 kcal/mol.[25] The backbone conformation differs dramatically among these structures, suggesting that mellitin may assume different forms if guided by the local environment. This appears to be the case on anionic interfaces where, possibly, the folded form of mellitin forms intervesicle contacts through which phospholipids exchange.[26]

In short, the topological flexibility suggested for PxB, and possibly many other peptides, does not contradict the conventional view that a conformationally fixed structure guides specific receptor−ligand interaction. Rather, the topological flexibility in the higher-order structures may be a critical design element that enables PxB, and possibly numerous other peptides, to perform a range of microscopically distinct functions guided by the gradients of the local environments presented at biological interfaces.

(24) Srimal, S.; Surolia, N.; Balasubramanian, S.; Surolia, A. *Biochem. J.* **1996**, *315*, 679−686.
(25) Lee, J.; Scheragga, H. A.; Rackovsky, S. *Biopolymers* **1998**, *46*, 103−115.
(26) Cajal, Y.; Jain, M. K. *Biochemistry* **1997**, *36*, 3882−3893.

Experimental Section

Purification of Polymyxin B. Polymyxin B from Sigma was purified by reverse phase HPLC on a Isco or Rainin HPLC with a Zorbax ODS semipreparative column (210 × 10 mm, 7 μm particle size). Aliquots of 100 μL from a stock solution of 25 mg/mL PxB in water were injected and eluted at a flow rate of 3.2 mL/min using a gradient method from 25% to 29% A in 40 min (A = acetonitrile/H_2O/TFA 90:10:0.1%; B = H_2O/acetonitrile/TFA 90:10:0.1%). After each injection, the gradient was increased to 100% B in 5 min and maintained in this conditions for 10 min, to wash any nonpeptidic impurities. The solvents were degassed by vacuum prior to use. The presence of premixed acetonitrile and water in both phases is a necessary precaution to avoid formation of air bubbles on mixing at this high flow rate. The eluted sample was monitored by UV at 220 nm. PxB eluted with a retention time of 16 min, and only the central part of the PxB peak was collected. Impurities appeared as two small peaks of lower retention times. The acetonitrile was removed using a high vacuum rotary evaporator, and the sample was then lyophilized. Purified PxB was >99.9% pure by the analytical HPLC (Zorbax analytical column, 250 × 4.6 mm, 7 μm, elution with water−acetonitrile−0.1%TFA mixtures). The identity of purified PxB was assessed by electrospray mass spectrometry (expected mass M = 1205; found: 1206 $(M + H)^{+1}$, 1227 $(M + Na)^{+1}$, 624 $(M + 2H/2)^{2+}$, 614 $(M + H + Na/2)^{2+}$).

Size-Exclusion Chromatography of PxB. The state of aggregation of PxB in solution was determined by high performance size-exclusion chromatography on a Superdex Peptide HR 10/30 column of 100−7000 molecular weight range (Pharmacia Biotech) connected to a FPLC system (Pharmacia). Samples were eluted with 10 mM Tris buffer/0.2 M NaCl, pH 8.0. The flow rate was 0.5 mL/min, and detection was set at 220 nm. Several pure peptides of known molecular weight were injected as standards in the same conditions: polymyxin B nonapeptide (MW = 963.1), GSAN21 (MGCLGNSKTEDQRNEEKAQRE, MW = 2423), GSAC14 (DIIQRMHLRQYELL, MW = 1870), and KAA7 (KAAKAAKAAKAAKAAKAAKAAKAA, MW = 2178) were used for calibration. Peptides (5−10 μg in 5−10 μL) were injected from stock solutions in water. PxB was injected in the same conditions and eluted with a retention time that corresponds to the molecular weight of the monomer form; thus it does not seem to aggregate in solution.

CD Spectroscopy. The spectra were recorded on a Jasco J700 spectropolarimeter in 1 or 10 mm cells with 1 mm slit-width. Wavelengths from 260 to 190 nm were scanned at a rate of 20 nm/min. Typically three to five scans were averaged, and the spectrum of buffer or vesicle blanks was subtracted. For CD spectra in aqueous TFE, the peptide concentration was typically between 100 and 150 μM. The pH and TFE concentration dependence was obtained from solutions prepared in the buffer at the indicated pH. The contribution of the scattering artifact was judged to be negligible because the molar ellipticity was the same at both 1 and 10 mm path lengths. All CD spectra in TFE/H_2O were smoothed to reduce noise.

NMR Spectroscopy. NMR samples were prepared using purified PxB, and the concentration was determined by mass. The pH of the distilled water used to dissolve PxB was adjusted to approximately 3.5, prior to dissolution, by addition of dilute HCl; no buffer was used to maintain the pH. Deuterated trifluoroethanol (TFE) was obtained from Cambridge Isotopes, and the TFE percentage in mixed solvents was measured by volume. NMR sample concentrations were between 5 and 6 mM in water and either TFE-d_3 (50%TFE) or TFE-d_2 (CF_3-CD_2OH) for the samples in 30 and 70% TFE.

All NMR spectra were obtained on a Bruker DRX 400 NMR spectrometer operating at a proton frequency of 400 MHz. For all NMR experiments, the large water signal was suppressed by presaturation, where the water resonance is selectively irradiated for one second prior to acquisition of each transient,[27] which also serves as the relaxation delay for the other resonances. For 1D ^{1}H spectra, a total of 64−128 transients were accumulated, each with 32K complex points (16K real) and an effective sweep width of 5600 Hz (14 ppm) centered at the water resonance (3 s acquisition time per transient).

(27) (a) Campbell, I. D.; Dobson, C. M.; Ratcliffe, R. G. *J. Magn. Reson.* **1977**, *27*, 455−463. (b) Molday, R. S.; Englander, S. W.; Kallen, R. G. *Biochemistry* **1972**, *11*, 150−158.

Interproton Distances

Distances were determined using the two-spin approximation.[12] As a first step, a series of 2D NOE spectra were recorded with mixing times ranging from 50 to 400 ms. If a single molecular correlation time is assumed (i.e. that all protons experience the same type and frequency of molecular motion), then an unknown distance, r_{unk}, can be estimated by comparing the initial build-up rate of the cross-peak intensity for this interaction, σ_{unk}, to the initial rate measured for the known distance, σ_{known}, using eq 1[12]

$$r_{unk} = r_{known} * (\sigma_{known}/\sigma_{unk})^{1/6} \quad (1)$$

where r_{known} is the distance between the two H^γ methylenes of Dab-4, assumed to be 1.75 Å.[13]

Dihedral Angles. Estimates of dihedral angles were obtained from amide vicinal coupling constants, $^3J_{HN\alpha}$, measured from the normal proton spectrum and/or the 2D J-resolved spectrum. These coupling constants were converted to dihedral angles using the Karplus relation given by eq 2[9]

$$^3J_{HN\alpha} = 6.4 \cos^2\theta - 1.4 \cos\theta + 1.9 \quad (2)$$

Mass Spectrometry. Electrospray mass spectra were taken on a Autospec (Micromass, Manchester, UK) with a flow rate of 10 μL/min and a mass range of 200−1500 daltons. These experiments were kindly carried out by Dr. Gordon Nicol.

Simulated Annealing. All calculations were done on a Silicon Graphics Indigo work station using the Discover and InsightII packages (Biosym Technologies). Parameters for lysine were used for Dab. Simulations were done in vacuo using a CVFF force field without Morse potentials, charges, or cross terms. The basic protocol for simulated annealing has been described elsewhere.[16] Interproton distances and dihedral angle restraints were introduced by adding a forcing potential that adds a penalty term to the energy if the distances and/or angles differ significantly from the NMR data. This potential is zero for distances and/or angles between the defined lower and upper limits and increases quadratically as these limits are exceeded. Chirality restraints were similarly introduced; a penalty energy term is added if the chirality of any residue is violated. To start the simulated annealing schedule, the molecular coordinates are randomized. The first stage consists of high-temperature minimization (1000 K) with minimal contribution from restraint forcing potentials, using 100 steps of steepest descent followed by 500 steps of conjugate gradient minimization. This is followed by 50 ps of restrained molecular dynamics at 1000 K consisting of three phases: (a) the distance and angle force constants are scaled to their full values of 30 kcal/Å^2 mol and 20 kcal/deg^2 mol respectively over 30 ps, (b) the covalent and chiral force constants are scaled to 15% of full value over 10 ps, and (c) the force constants for nonbond interactions are increased while doubling distance and angle force constants over 10 ps. In the next stage of restrained molecular dynamics, the molecule is gradually cooled in five steps of 2 ps, without changing any force constants. The molecule is then minimized at 300 K using 100 steps of steepest descent followed by 500 steps of conjugate gradient minimization. Finally, all force constants are returned to their full value, and the molecule is minimized using 100 steps of steepest descent followed by 1500 steps of conjugate gradient minimization. This procedure is repeated to generate 20 structures, each from a new, random array of atoms for each structure. Since absolute energies for calculated structures in vacuo are difficult to interpret, it is desirable to obtain a reasonable estimate for the apparent global minimum energy for the peptide. To provide such an estimate, a second set of 20 structures was generated from simulated annealing with a final phase added at the end where an *unrestrained* energy minimization is performed on the molecule. Ramachandran plots were generated for each structure by using the coordinates as input for the PROCHEK from the CCP4 (Collaborative Computational Project, Number 4, *Acta Crystallogr.* **1994**, *D50*, 760−763) suite of programs to generate the Ramachandran plots. Both the N- and C-terminal residues were excluded from the Ramachandran plots.

Docking and Energy Minimization. The NMR structure shown in Figure 4 was used as a starting structure for docking several anionic phosphoesters to the *N*-acetylated polymyxin (C2-PxB) or its acetylated 3−10 analogue (C2-octapeptin). Molecular mechanics calculations suggested the presence of two distinct and specific phosphoester sites. Docking simulations using extended AMBER force field were carried out using a Monte Carlo docking algorithm,[28] FLO96/QXP (available from Thistlesoft, P.O. Box 227, Colebrook, CT06021; telephone: 860-379-5502; e-mail: cmcma@ix.netcom.com). Minimized energies are reported relative to the global minimum of the phosphodiester ligand minimized in the absence of the C2-PxB or octapeptin cavity. The structure of C2-PxB was unrestrained except for residues 6 and 7 which were constrained by a penalty of 20 kJ/Å^2 (4.8 kcal/Å ^{2}) for deviations beyond 0.5 Å of the starting geometry. The minimization algorithm uses a distance-dependent dielectric (4.0*r*). In the absence of explicit solvent, the binding energies will clearly overemphasize the electrostatic interaction of PxB with the phosphodiester ligand. However, the relative values provide qualitative insights into potential modes of the phosphodiester binding. Monte Carlo docking simulations were conducted for each ligand by directing the ligand to dock on five different regions that encompass the entire surface of C2-PxB for a total of 2500 docking steps for each ligand. Docking of two ligands into the two cationic sites A and B were conducted by sequential Monte Carlo docking routines into site B and site A. Simultaneous simulated annealing of both ligands was used to obtain a final doubly occupied structure.

Calorimetric Titrations. Isothermal calorimetric titrations of phospholipid vesicles with PxB or NP were carried out using a VIP isothermal calorimeter (Microcal Inc.) with a 1.43 mL reaction volume. Each addition represents 1 nmol peptide in 2 μL of stock solution successively added every 240 s. Control experiments showed that the heat changes shown here are not due to dilution or a pH difference.

Acknowledgment. This work was supported by Grant GM29703 from the National Institutes of Health. We thank Dr. Gordon Nicol for the mass spectrometry results and Dr. Brian Bahnson for assistance with generation of the Ramachandran plots.

Supporting Information Available: NMR TOCSY and NOESY spectra, Experimental details for NMR experiments and analysis as well as computational methods (PDF). This material is available free of charge via the Internet at http://pubs.acs.org.

JA992376M

(28) McMartin, C.; Bohacek, R. S. *J. Comput.-Aided Mol. Des.* **1997**, *11*, 333−344.
(29) Lee, B.; Richards, F. M. *J. Mol. Biol.* **1971**, *55*, 379−400.